Cite this article
Rubaka C, Gathirwa JW, Malebo HM *et al.* (2023)
Chitosan-coated liposomes of *Carissa spinarum* extract: synthesis, analysis and antipneumococcal potency.
Bioinspired, Biomimetic and Nanobiomaterials **12(1)**: 12–23,
https://doi.org/10.1680/jbibn.22.00046

Research Article
Paper 2200046
Received 12/08/2022; Accepted 08/02/2023
First published online 16/02/2023

Bioinspired, Biomimetic and Nanobiomaterials

ice Publishing

Chitosan-coated liposomes of *Carissa spinarum* extract: synthesis, analysis and antipneumococcal potency

Clarence Rubaka MSc
PhD student, Global Health and Biomedical Sciences, Nelson Mandela African Institution of Science and Technology, Arusha, Tanzania; Assistant Lecturer, Department of Chemistry, St John's University of Tanzania, Dodoma, Tanzania (Orcid:0000-0002-7620-0143) (corresponding author: rubaka.ccc@gmail.com)

Jeremiah Waweru Gathirwa PhD
Principal Research Scientist, Center for Traditional Medicine and Drug Research, Kenya Medical Research Institute, Nairobi, Kenya (Orcid:0000-0002-8059-4990)

Hamisi M. Malebo PhD
Professor, Unesco National Commission of the United Republic of Tanzania, Dar-es-salaam, Tanzania (Orcid:0000-0001-6081-9120)

Hulda Swai PhD
Professor, Global Health and Biomedical Sciences, Nelson Mandela African Institution of Science and Technology, Arusha, Tanzania (Orcid:0000-0003-2180-8300)

Nicole Remaliah Samantha Sibuyi PhD
Research Scientist, DSI/Mintek Nanotechnology Innovation Centre – Biolabels Node, Department of Biotechnology, University of the Western Cape, Cape Town, South Africa (Orcid:0000-0001-7175-538)

Askwar Hilonga PhD
Professor, Material Science and Engineering, Nelson Mandela African Institution of Science and Technology, Arusha, Tanzania (Orcid:0000-0002-2938-5149)

Admire Dube PhD
Professor, Infectious Diseases Nanomedicine Laboratory, Department of Pharmaceutical Sciences, Faculty of Natural Sciences, University of the Western Cape, Cape Town, South Africa (Orcid:0000-0002-5684-6094)

In the present study, a chitosan-coated *Carissa spinarum*-polyphenol-loaded liposome (LipCsP-chitosan) nanocarrier was fabricated for the delivery of *C. spinarum* polyphenols (CsPs) to improve the bioavailability and antipneumococcal potential of CsPs against *Klebsiella pneumoniae*. LipCsP-chitosan was synthesized using the ion gelation method and characterized by using a Malvern Zetasizer and Fourier transform infrared (FTIR) spectroscopy. CsP encapsulation and release kinetics were investigated. The antipneumococcal activity of the nanoformulations was assessed using agar-well diffusion and microdilution assays. LipCsP-chitosan exhibited a hydrodynamic size and a zeta potential of 365.22 ± 0.70 nm and +39.30 ± 0.61 mV, respectively. The encapsulation efficiency of LipCsP-chitosan was 81.5%. FTIR analysis revealed interactions of the liposomes with chitosan and CsPs. A biphasic CsP release profile followed by a sustained-release pattern was observed. LipCsP-chitosan presented a higher bioaccessibility of polyphenols in the simulated gastric phase (74.1 ± 1.3%) than in the simulated intestinal phase (63.32 ± 1.00%). LipCsP-chitosan had a relative inhibition zone diameter of 84.33 ± 2.51% when compared with CsPs. At a minimum inhibitory concentration of 31.25 mg/ml, LipCsP-chitosan reduced the viability of *K. pneumoniae* by 57.45 ± 3.76% after 24 h. The results obtained from this study offer a new approach to the utilization of LipCsP-chitosan as nanocarriers for candidate antipneumococcal agents.

Keywords: anti-bacterial/chitosan/nanoparticles/polymers/UN SDG 3: Good health and well-being

Notation

C_0	initial total phenolic content of polyphenols before release by nanoformulations
$C_{digesta}$	concentration of *Carissa spinarum* polyphenols (CsPs) in the mixed micelle phase
C_i	initial concentration of CsP
C_t	cumulative amount of polyphenols released by the nanoformulation after an elapsed time t
K	rate constant
K_H	Higuchi constant
K_{KP}	Korsmeyer–Peppas constant
N	exponential factor that predicts the Korsmeyer–Peppas model
t	time
Z_P	zeta potential

1. Introduction

One of the serious health challenges that will have to be tackled in the years to come is the increasing antimicrobial resistance of bacterial pathogens.[1] It has been predicted that by 2050, deaths caused by antimicrobial resistance will widely outnumber those caused by cancer today.[2] Therefore, there is an urgent demand for the development of novel and effective antimicrobial agents. Several approaches to overcoming bacterial drug resistance have been developed, with the use of drug carriers such as nanoparticles seeming to be one promising approach.[3]

indeed, drug nanocarriers were demonstrated to protect antimicrobial agents and enable them to reach the targeted biological site at an optimal concentration and increased bioavailability; with a desirable pharmacological response and reduced side effects.[4] Thus, the application of nano-based antibacterial materials is considered a plausible approach that can help combat the antimicrobial resistance problem by providing an alternative non-resistance mechanism against bacteria.[5]

In general, nano-based antimicrobial delivery systems can interact with microorganisms through two mechanisms to improve their performance: by fusing with the microbial cell wall or membrane and releasing their payload within the cell wall or membrane, or by adsorption into the cell wall and providing an antibiotic depot that continuously releases drug molecules. Both result in the diffusion of nanocarriers and their cargoes into the interior of the cell.[6] Moreover, drug-loaded nanoparticles can enter host cells through endocytosis, followed by release of the loaded drugs, which in turn destroys the microorganisms from within.[7]

Due to insufficient vaccine coverage of all pneumococcal serotypes and a high percentage of antibiotic-resistant strains, the search for alternative treatments of bacterial pneumococcal infections is of paramount importance.[8] One of the particular traits of bacterial pneumococcal pathogens is the presence of choline residues in the teichoic acids of their cell wall.[9] These choline residues act as binding ligands for choline-binding proteins (CBPs), surface proteins to which bacterial and phage peptidoglycan hydrolases in pneumococcal systems typically belong.[10] Because of the specificity of such ligands, choline and CBPs have emerged as targets for novel antipneumococcal drug design.[11]

Engineering cell membrane mimetics could be a suitable target for these pathogens. Cellular mimetics based on lipid nanoparticles have been mimicking the cellular membrane due to the presence of common features such as the lipid bilayer. Lipid-based nanoparticles could provide a plausible binding to the CBPs of *Klebsiella pneumoniae* strains. Liposomes are among the organic nanomaterials that have been widely used as versatile drug delivery vehicles for a decade, due to their biocompatibility. However, the use of liposomes alone is limited by their instability,[12] which is improved by coating liposomes with polymers.[13]

Liposome surface-based chitosan cationic impregnation adds to the repulsion force between nanoparticles and improves their stability and antimicrobial activity.[14] Vázquez *et al.*[15] synthesized chitosan nanoparticles derivatized with diethylaminoethyl groups (ChiDENPs) to emulate the choline residues in the pneumococcal cell wall and act as ligands for CBPs. The fabricated ChiDENPs released an antimicrobial enzyme against *Streptococcus pneumoniae*. The presence of chitosan in the ChiDENP nanocomposite improved the binding ability of the nanoparticles to the CBPs of the *S. pneumoniae* strain.

In this study, phosphatidylcholine was encapsulated in nanovesicles (liposomes) as a lipid biomaterial, *Carissa spinarum* polyphenols (CsPs) were encapsulated and CsP-loaded liposomes (LipCsPs) were coated with chitosan. The physicochemical properties of the fabricated nanosystem (chitosan-coated LipCsP (LipCsP-chitosan)) were characterized, and its antibacterial potential was tested against *K. pneumoniae.* The fabricated nanohybrid system is envisaged to interact with the microorganisms by fusing with their cell wall or membrane and releasing active CsPs, or adsorbing into the cell wall and then releasing the polyphenols, which will act as an antibacterial agent against *K. pneumoniae*.

C. spinarum is used both as food and as medicine in traditional African societies.[16] Its fruits and flowers are eaten as food,[16] while its bark, roots, branches and leaves are used to treat several ailments, including gonorrhea, diarrhea, syphilis, cough,[17] viral diseases,[18] chest pains[19] and worm infestation.[20] *C. spinarum* has been shown to also have anti-inflammatory, anticancer,[17] antioxidant[21] and purgative effects. The plant was reported to be rich in medicinal compounds such as polyphenols, which are responsible for treatment of several diseases.[22] Despite the potential exhibited by *C. spinarum* in the treatment of bacterial infections, the bioavailability of antibacterial compounds such as polyphenols limits its antibacterial efficacy. The bioavailability of polyphenols has been improved when integrated with several delivery systems.[23,24]

2. Materials and methods

2.1 Materials

The reagents and equipment used in this study included the following: sodium triphosphate, α-L-phosphatidylcholine, chitosan (Sigma-Aldrich, USA), nutrient broth (Biolab Merck, Darmstadt, Germany), a centrifuge machine (Heraeus Sepatech 1217, 15 revolutions per min (rpm), Hanau, Germany), a vortex (BenchMixer, Benchmark Scientific), a magnetic stirrer (FMH Instruments), a homogenizer (T 18 digital Ultra-Turrax, IKA), pH meters (XS Instruments; pH 2700, Eutech Instruments; Wirsam), a bath sonicator (Scientech ultrasonic cleaner), Fourier transform an infrared (FTIR)–near-infrared (NIR) spectrometer (Spectrum 400, PerkinElmer, Waltham, MA, USA), a probe sonicator (Sonopuls, Bandelin), a Nano ZS Zetasizer (Malvern, UK), plate reader (Polarstar Omega, BMG Labtech, Offenburg, Germany), a shaker (Belly Dancer, Stovall, Greensboro, NC, USA), an orbital shaker incubator (LM-530, Yihder), a biosafety cabinet (Labotec, Cape Town, South Africa), an incubator (Forma Scientific), alamarBlue (Invitrogen, USA), benchtop freeze dryers (VirTis 2K, 4K and 6K, SP Scientific, Gardiner, NY, USA) and glacial acetic acid (Cameron Chemical Consultants). Sodium cholate, pepsin, pancreatin and Triton X-100 were purchased from Chemicals & School Supplies Limited (Nairobi, Kenya).

2.2 CsP phytochemical extraction and screening

2.2.1 Collection and preparation of the medicinal plant

C. spinarum leaves were collected from Loliondo (Tanzania, Africa) between May and June 2019. The detached leaves were

packed in containers and sent to the Nelson Mandela African Institution of Science and Technology (NM-AIST) laboratory for further preparation. At the NM-AIST laboratory, the leaves were stored in a shaded, dry place for 1 month. After the leaves were thoroughly dry, they were ground into powder using a blender. The *C. spinarum* leaf powder was stored in a desiccator until it was used for extraction.

2.2.2 CsP extraction

The process of extraction was conducted at the African Technical Research Center analytical laboratory (Arusha, Tanzania). Powdered leaves (200 g) were soaked in 500 ml of methanol and left for 2 days. After 2 days, the macerated leaves were subjected to rotary evaporation to form a crude methanol extract. The crude extract was filtered through Whatman number 1 filter paper to remove some residual particles.

The filtered product was then concentrated by using a rotary evaporator. The extraction procedures were repeated in chloroform, petroleum ether and water to produce chloroform, petroleum ether and water (aqueous) extracts, respectively. The four extracts (methanol, chloroform, petroleum ether and water extracts) were stored in refrigerators at 4°C until further analysis.

2.2.3 Qualitative phytochemical analysis

Phytochemical analysis was conducted following the method developed by Sonam *et al.*[25] to test for the presence of *C. spinarum* phytoconstituents, including alkaloids, flavonoids, phenols, terpenoids, steroids, coumarins, resins, tannins, xanthoproteins, quinines, carboxylic acid, oxalates, carbohydrates, glycosides, proteins and saponins.

2.3 Extraction and analysis of polyphenols

2.3.1 Microwave-assisted extraction of polyphenols and estimation of the total phenolic content

A household microwave was modified by integrating a magnetic stirrer and a water condenser with it. Powdered *C. spinarum* leaves (50 g) were soaked in 200 ml of distilled water in a 500 ml round-bottomed flask. The flask was then irradiated in the microwave for 30 min. After 30 min, the extract was filtered using Whatman number 1 filter paper. The filtrate was fixed in a rotary evaporator to concentrate polyphenols in a methanol extract. The extract in the water was freeze-dried.

The total phenolic content (TPC) was measured by using the Folin–Ciocalteu method according to a previous study[26] with slight modifications. Briefly, 1 mg of the extract was dissolved in 1 ml of distilled water. Then, 5 ml of 1% Folin–Ciocalteu reagent was added to 1 ml of the extract. To this mixture, 5 ml of 7.5% sodium carbonate was added, and then the mixture was incubated at 25°C for 20 min. The absorbance was measured at 760 nm, and the TPC was expressed as milligrams of gallic acid equivalents (GAE) per gram.

2.3.2 Synthesis of liposomes and encapsulation of CsPs

LipCsPs were prepared by using the ethanol injection method, following the protocol developed by Cheng *et al.*,[27] with some modifications. Briefly, 50 mg of phosphatidylcholine was mixed with 10 ml of absolute ethanol. Then, 20 mg of *C. spinarum* leaf extract enriched in polyphenols was added to 20 ml of preheated distilled water at 60°C.

The phosphatidylcholine-in-ethanol mixture was slowly added to an aqueous medium containing CsP extract and stirred at 60°C for 40 min. After 40 min, the ethanol was removed by rotary evaporation, and the lipid suspension was then sonicated for 30 min and homogenized. The resulting LipCsPs were kept at 40°C for further analysis.

2.3.3 Preparation of chitosan-coated LipCsPs

Briefly, phosphatidylcholine (100 g) was mixed into 15 ml of ethanol to form a lipid–ethanol mixture. The mixture contains chitosan (40 mg), sodium triphosphate (10 mg) and extract (20 mg), which was dissolved in 1% acetic acid and then subjected to water bath sonication. To this mixture, ethanol was added dropwise. Probe sonication at 50% amplification for 30 min was conducted, and the mixture was centrifuged at 15 000 rpm at 4°C for 15 min. The pellets of LipCsP-chitosan were collected and freeze-dried.

2.3.4 Encapsulation efficiency measurement

The liposome solution was dissolved in acetone at a ratio of 0.5:1 and then centrifuged at 15 rpm for 30 min. The supernatant was removed and put in oven at 60°C for removal of the solvent. The remaining substance was added to 5 ml of distilled water, and the TPC was measured using the Folin–Ciocalteu method.[26] Before performing the Folin–Ciocalteu method, 1 ml of 0.06% Triton X-100 was added to the samples to solubilize the phosphatidylcholine.

Encapsulated CsPs were obtained as the difference between the value of TPC present in CsP samples alone and that which remained after removing acetone. The encapsulation efficiency (EE) was calculated using the following equation:

$$\text{EE}\ (\%) = \frac{\text{phenols inside}}{(\text{phenols inside} + \text{phenols outside})} \times 100 \quad (1)$$

The term 'phenols inside' denotes CsPs inside the liposomes, and 'phenols outside' represents the CsPs in the supernatant.

2.4 Characterization of nanoformulations

2.4.1 Particle size and ζ potential measurements

The mean particle sizes and zeta potentials of the nanoparticle formulations were determined using a Malvern Zetasizer. The nanoparticles were appropriately diluted with deionized water to

allow the light-scattering intensity to be within the sensitivity range of the instrument.

2.4.2 FTIR spectroscopy

The infrared (IR) spectra of the liposomal formulations were obtained using a PerkinElmer Spectrum 400 FTIR–NIR spectrometer within the wave number range 4400–400 cm^{-1}. The spectra were collected using 24 scans and at a 2 cm^{-1} resolution to determine the functional groups of the formulations.

2.5 Release of CsPs from liposomes

An in *vitro* release experiment was performed using the method described by Omwoyo *et al*.,[28] with some modifications. Twenty milligrams of the liposomal formulation was ultracentrifuged at 15 000 rpm for 20 min. The supernatant was then discarded, and the pellets were further dispersed in a pH 7.4 buffer solution and then placed in a shaker maintained at 37°C to mimic body conditions. The liposomal formulations were sampled after different test time intervals (1, 2, 3, 4, 5, 6, 7, 8, 12 and 24 h) for determination of TPC, and the release kinetics were expressed as cumulative percent release against time.

2.5.1 Mathematical modeling

The mathematical models used to study the CsP release kinetics used in this study are the zero-order, first-order, Higuchi, Hixson–Crowell and Korsmeyer–Peppas models (Table 1). The correlation coefficient (R^2) and the release exponent (N) were used to determine the best-fit kinetic model and the mechanism of the CsP release.

2.6 Gastrointestinal digestion

2.6.1 Simulated mouth fluid

A simulated salivary fluid containing mucin (30 mg/ml) was prepared following the method developed by Pool *et al*.[29] Each sample (3 ml) was mixed with simulated saliva fluid (3 ml) and preheated to 37°C. The pH of the resulting mixture was adjusted to 6.8 with 50 mM sodium hydroxide (NaOH), and then the mixture was shaken at 90 rpm for 10 min at 37°C to mimic oral conditions.

2.6.2 Simulated gastric fluid

Simulated gastric fluid (SGF) was prepared by mixing 0.03 M sodium chloride (NaCl), 0.16 M hydrochloric acid (HCl) and pepsin (3.2 mg/ml) and incubating the mixture at 37°C. SGF was added to 3 ml of the sample from the simulated mouth fluid. The pH of the mixture was adjusted to 2.5, and the mixture was shaken at 100 rpm for 2 h to mimic digestion in the stomach.

Table 1. Mathematical models for studying the drug release kinetics

Kinetic model	Equation
First-order model	$\log C_t = \log C_0 - Kt/2.303$
Zero-order model	$C_t = C_0 + Kt$
Higuchi model	$C_t = K_H \times t^{1/2}$
Korsmeyer–Peppas model	$\log(C_t/C) = \log K_{KP} + N \log t$

2.6.3 Simulated intestinal fluid

Samples from the simulated gastric model were diluted with phosphate-buffered saline (PBS; 10 mM, 12 ml, pH 6.5) and shaken at 37°C for 10 min. The solution was then adjusted to pH 7.0. Simulated small intestinal fluid containing pancreatin (24 mg/ml, 2 ml), bile extract solution (50 mg/ml, 2.8 ml) and saline solution (0.5 M calcium chloride ($CaCl_2$) and 7.5 M sodium chloride, 1.2 ml) was added into the digestion samples.

The pH of each digestion sample was maintained at pH 7.0 by the addition of 50 mM sodium hydroxide.

2.7 Determination of the bioaccessibility of CsPs

A total of 200 l of the raw digest was extracted at various stages of digestion (gastric and intestinal phases) and used for TPC analysis. To fracture the liposomal membranes completely, samples were diluted with a solution containing 1% Triton X-100 and adjusted to pH 5. Subsequently, the sample was centrifuged at 13 400 rpm and 4°C for 30 min. The supernatant was carefully collected and considered to be the 'micelle' fraction, in which the bioactive compounds were solubilized. The amount of CsPs present was quantified by using the Folin–Ciocalteu method, and bioaccessibility was calculated according to the equation

$$\text{Bioaccessibility } (\%) = \frac{C_{\text{digesta}}}{C_i} \times 100 \quad (2)$$

where C_{digesta} and C_i are the concentrations of CsPs in the mixed micelle phase and the initial concentration, respectively.

2.8 Nanoformulation stability in a simulated gastrointestinal environment

The stability of the nanoformulations in a simulated gastrointestinal environment was evaluated by measuring the zeta potential and hydrodynamic size of the samples using the Zetasizer Nano Z equipment (Malvern Instruments) at 20°C.

2.9 Antibacterial activity

2.9.1 Collection and preparation of inocula

The *K. pneumoniae* strain was an in-kind gift from the DSI/Mintek Nanotechnology Innovation Centre – Biolabels Node (Department of Biotechnology, University of the Western Cape) and was purchased from the American Type Culture Collection (Manassas, VA, USA). The microorganism was inoculated on agar nutrient agar plates and incubated for 24 h at 37°C. After incubation, the plates were stored in a refrigerator at 4°C for antimicrobial tests. Inoculated microorganisms were picked from nutrient agar by using a wire loop and added to nutrient broth and adjusted to 0.5 McFarland standard (0.08–0.10 at 600 nm).

2.9.2 Agar-well diffusion assay

The microorganisms were cultured until they reached 0.5 McFarland and diluted to approximately 10^6 colony-forming units

(CFU)/ml in fresh nutrient broth. Then, 100 µl of diluted cultures was spread on the surface of nutrient agar plates. For treatments, 70 µl of nanoformulations and the CsP extracts were added into the wells (8 mm in diameter) made on the agar plates. Ciprofloxacin at 10 µg/ml was used as positive controls. After incubation for 24 h at 37°C, all plates were examined for any zones of inhibition around the wells.

Antibacterial activity was determined by measuring the zones of inhibition against test microorganisms. The experiment was repeated three times. The antimicrobial activity was expressed as percent relative inhibition zone diameter (RIZD), as previously described,[22] using the equation

$$\%\ \mathrm{RIZD} = (\mathrm{IZD\ sample} - \mathrm{IZD\ negative\ control}) \times \frac{100}{(\mathrm{IZD\ antibiotic\ standard})} \quad (3)$$

2.9.3 Microdilution alamarBlue assay

The microdilution alamarBlue assay was used to assess the susceptibility of *K. pneumoniae* to the nanoformulations. In a 96-well plate, the concentrations of the nanoformulations were serially diluted in the range from 500 to 31.25 mg/ml. In each well, 100 µl of 1×10^6 CFU/ml *K. pneumoniae* was added, and the plate was incubated at 37°C for 24 h.

The minimum inhibitory concentration (MIC) was recorded as the lowest concentration of treatments that visually inhibited 100% of growth. Following that, 10 µl of the alamarBlue dye reagent was added to each well and incubated at 37°C for 3 h. The growth of the microorganisms was determined by absorbance at 570 nm on a BMG microplate reader, and cell viability was calculated by using the equation

$$\%\ \mathrm{Viability} = \frac{\mathrm{absorbance\ of\ nanoformulation\text{-}treated\ cells}}{(\mathrm{absorbance\ of\ control\ cells})} \times 100 \quad (4)$$

2.10 Statistical analysis

Statistical analysis was performed using analysis of variance, with the computations performed with the software program Origin 2019 (64-bit), and Fisher's least significant difference (LSD) was used to compare treatment means at the $P = 0.05$ level of significance.

3. Results and discussion

3.1 CsP phytochemical analysis

Various tests indicated the presence of different vital phytochemicals in the different extracts of *C. spinarum*; the phytochemicals are summarized in Table 2. The majority of phytochemicals were found in the methanol and water extracts, with only the tannins and glycosides extractable by chloroform. The phytoconstituents were mostly distributed in a polar solvent than in a non-polar solvent and fall in the polyphenol classes. These bioactive phytochemicals are the source of the therapeutic potential of medicinal plants and are useful in the treatment of several diseases.[17]

The TPC of the methanol and water extracts as determined by using the Folin–Ciocalteu method was expressed as milligrams

Table 2. Phytochemical screening of *C. spinarum* leaf extract

Phytochemicals	Type of test	Methanol extract	Aqueous extract	Petroleum ether extract	Chloroform extract
Alkaloids	Mayer's test	+	+	–	–
	Wagner's test	+	–		
Flavonoids	Ammonia reduction test	+	+	–	–
Phenols	Ferric chloride test	+	+	–	–
Terpenoids	Salkowski's test	+	–	–	–
Steroids	Salkowski's test	+	+	–	–
Coumarins	Sodium hydroxide test	+	+		
Resins	Copper sulfate test	–	–	–	–
Tannins	Ferric chloride test	+	+	–	+
Xanthoproteins	Nitric acid + ammonia test	–	–	–	–
Quinones	Alcoholic potassium hydroxide (KOH) test	–	–	–	–
Carboxylic acid	Effervescence test	–	–	–	–
Oxalates	Acetic acid test	+	–	–	–
Carbohydrates	Fehling's test	+	+	–	–
Glycosides	Keller–Killiani test	+	–	–	+
Proteins	Ninhydrin test	–	–	–	–
Saponins	Froth test	+	+	–	–

+, present; –, absent

GAE per gram of CsP dry weight (mg GAE/g). The Folin–Ciocalteu method is based on the transfer of electrons from phenolic compounds to phosphomolybdenum–phosphotungstic acid complexes in an alkaline medium to form blue-colored complexes whose absorbance can be measured spectrophotometrically at 760 nm.

The TPC measured at the maximum concentration (1 mg/ml) confirmed that the methanol extract had a high polyphenol content compared with the water extract (Table 3) – that is, 362.00 ± 1.00 mg GAE/g against 348.00 ± 1.53 mg GAE/g. *C. spinarum* contains phytochemicals, which are responsible for treating several diseases as practiced in traditional medicine. These bioactive phytochemicals in *C. spinarum* present this plant species as a potential pharmaceutical source that can be developed into useful drugs for the treatment of diseases.

Terpenoids were reported to exhibit antimicrobial activities by rupturing the microbial cell membrane and impeding the function of ion (sodium (Na^+), potassium (K^+), calcium (Ca^{2+}) or chloride (Cl^-) ion) channels. Thymol, a terpenoid commonly found in essential oils, was also reported to form a hydrogen bond with the active sites of target enzymes and ultimately inactivate the enzymes.[30] The antimicrobial activity of tannins was due to their ability to precipitate proteins, as well as their inhibition of metabolic processes such as oxidative phosphorylation.[31]

Flavonoids also elicit anti-inflammatory, antimicrobial and antioxidant activities. The antioxidant and chelating actions of flavonoids, which are demonstrated to enhance the antimicrobial activity of phytochemicals, are attributed to the hydroxyl group present in many polyphenols.[32] Saponins are bioactive antibacterial agents associated with the ability to form pores in the microbial cell membrane, thereby giving the toxic material free access to cell.[33] Alkaloids are credited as a good source of many drugs and destroys microbes by intercalating into their deoxyribonucleic acid.[22]

3.2 Synthesis and characterization of nanoformulations

3.2.1 Particle size, zeta potential, polydispersity index and EE

The characteristics of nanoliposomal formulations in terms of particle size, polydispersity index (PDI), zeta potential and EE were investigated, and the results are indicated in Table 4. The hydrophilic liposomes entrapped CsPs at 81.07 ± 2.5% in LipCsP-chitosan and at 66.11 ± 1.11% in the uncoated liposomes (LipCsPs). The high EE of LipCsP-chitosan was most likely due to the interaction of CsPs with both chitosan and the lipid bilayer.

These findings are consistent with the findings of Sebaaly *et al*.,[34] who proposed that coating liposomes with chitosan allows polyphenol moieties to interact with chitosan, increasing the EE. However, the positively charged drug competing with the positively charged functional group of chitosan when they bind electrostatically with the negatively charged group of phospholipids reduces the EE.[34]

The effect of coating the cationic capping agent was observed in this study, which indicated that coating the surface of liposomes with chitosan changed their physical properties, including the size and charge of the nanoparticles. The hydrodynamic diameter of LipCsPs was 176.17 ± 1.05 nm, which increased to 365.22 ± 0.70 nm due to the addition of chitosan in LipCsP-chitosan. The PDI values of the nanoliposomal systems remained below 0.4, which indicated a less pronounced tendency to aggregation.

The negative zeta potential of the LipCsP surface can be explained by the inherent composition of soybean lecithin that creates the bilayer of the liposomes. By electrostatic attraction, the positively charged amine group on chitosan interacted with the negatively charged phosphate group on the liposomes and was adsorbed on the liposomal surface. The adsorption of chitosan amplified the density of positive charge and made the zeta potential positive.[35]

Table 3. TPC (mg GAE/g) of *C. spinarum* leaf extracts

Sample	1.25 mg/ml	0.25 mg/ml	0.5 mg/ml	1 mg/ml
Methanol extract	362.00^{d} ± 1.00	365.00^{c} ± 1.00	368.00^{b} ± 1.20	373.00^{a} ± 1.52
Water extract	348.33^{h} ± 1.53	350.5^{g} ± 0.50	354.33^{f} ± 0.58	357.50^{e} ± 0.50

Note: values reported as mean ± standard deviation; $n = 3$. Means followed by dissimilar letters in a row are significantly different from each other at $P \leq 0.05$ according to Fisher's LSD

Table 4. Particle sizes, PDIs and zeta potentials of the nanoformulations

Formulation	Size: nm	PDI	Z_P: mV	EE: %
LipCsP-chitosan	365.22 ± 0.70	0.351 ± 0.00	+39.30 ± 0.61	81.07 ± 2.5
LipCsPs	176.17 ± 1.05	0.345 ± 0.00	–45.37 ± 0.78	66.11 ± 1.11

Note: LipCsPs, *C. spinarum*-polyphenol-loaded liposomes; LipCsP-chitosan, chitosan-coated LipCsPs. Values are reported as mean ± standard deviation; $n = 3$

The charge of LipCsPs changed from a negative value (−45.37 ± 0.78 mV) to a positive value (+39.30 ± 0.61 mV), as shown in Table 4. The study by Abosabaa *et al.*[36] reported that the increased zeta potential of chitosan-coated liposomes due to their cationic character can be used as an indication of successful coating. The greater the zeta potential magnitude, the greater the repulsion between particles and, thus, the more stable the colloidal dispersion.

Based on the value of the ζ potential obtained in this study, nanoliposomal systems had a minimal tendency to aggregate and were well stabilized in a colloidal environment since their ζ potential was greater than ±30 mV. Similar findings reported by Baranauskaite *et al.*[37] addressed the notion that zeta potential values higher than ±30 mV are indicative of a stable dispersion.

3.2.2 FTIR spectroscopy analysis

The FTIR spectra of CsPs, liposomes, chitosan and LipCsP-chitosan are shown in Figure 1. In the spectrum of chitosan (b in Figure 1), an absorption peak at 1653 cm^{-1}, corresponding to C=O stretching in amide I vibration, was observed. Also, bands corresponding to O–H and N–H stretching around the 3352 cm^{-1} region, a discrete absorption band at 2870 cm^{-1} due to C–H stretching that is typically present in polysaccharide IR spectra was observed. The primary amine functional group characterized with a bending vibration frequency at a wave number of 1578 cm^{-1} was present.

The liposomes in spectrum a in Figure 1(a), C–H stretching vibration, were clearly indicated by the presence of absorption bands at 2919 cm^{-1}. A strong signal also appeared at 1739 cm^{-1}, corresponding to C=O stretching vibration. Moreover, the peaks at 1467, 1236 and 1063 cm^{-1} were due to C–H bending, P=O and P–O–P stretching vibration, respectively. These findings were also

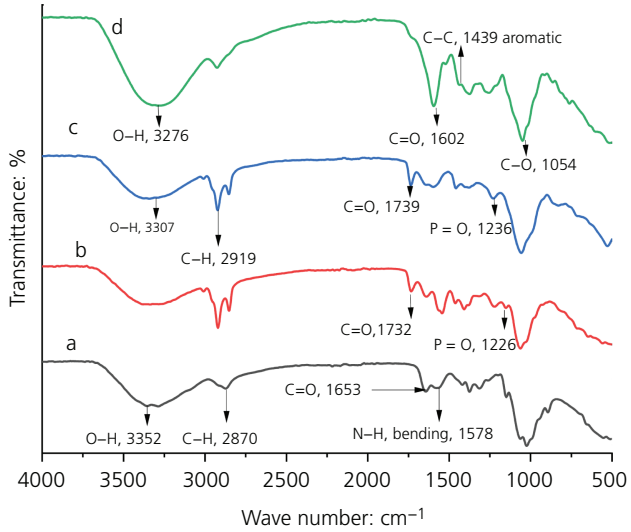

Figure 1. (a) FTIR analysis of liposomes, (b) chitosan, (c) CsPs and (d) LipCsP-chitosan

reported by Abosabaa *et al.*[36] Curve c in Figure 1 is the IR spectrum of CsPs, with the absorption peak at 3276 cm^{-1} reflecting OH stretching vibration ascribed to phenolic hydroxyl groups.[38,39] Flavonoid C–O functional groups and aromatic ring C–C were detected at 1602 and 1439 cm^{-1}, respectively, while C–O stretching vibration was detected at 1054 cm^{-1}. Curve d in Figure 1 is the FTIR spectrum of LipCsP-chitosan. The interaction of liposomes with chitosan was revealed by the disappearance of N–H primary amine (bending) in chitosan, which was previously reported.[36] Along this line, the stretch vibration frequency of O–H and N–H shifted from 3352 cm^{-1} to a lower vibration frequency of 3331 cm^{-1} due to hydrogen bonding between the liposomes and chitosan. Furthermore, the C=O vibration frequency of the liposomes shifted from 1739 cm^{-1} to a lower frequency of 1732 cm^{-1}. The changes in the absorption bands of the P=O group of liposomes from 1236 cm^{-1} to a lower frequency of 1226 cm^{-1} revealed the interaction between the CsP components and the liposomes.

3.3 In vitro release kinetics

The release kinetics of CsP from LipCsP-chitosan were studied at 37°C in PBS buffer (pH 7.4). The in vitro release behavior was observed in 48 h and recorded as percent cumulative release (Figure 2). A 100% drug release from the nanoformulation solution was achieved within 48 h. A biphasic release profile followed by a sustained-release pattern was observed. The mathematical kinetic model was also fitted to investigate the mechanism of CsP release from LipCsP-chitosan.

By applying equations for the kinetic models (Table 5), the rate constant (K) and correlation coefficient (R^2) were calculated, and the best-fit model was revealed by the highest R^2. The mechanism of release was also investigated by applying the Korsmeyer–Peppas model, where the value of the release component (N) of LipCsP-chitosan was $0.5 < N < 0.89$, demonstrating non-Fickian diffusion. This mechanism indicated that release was controlled by both the erosion and diffusion mechanisms. Primarily, the polymer swelled, forming a gelatinous mass, resulting in its relaxation followed by erosion and later by diffusion as the polymer became soluble and permeable.

3.4 Bioaccessibility of CsPs loaded in liposomes

Bioaccessibility is defined as the fraction of CsPs released from the liposomes that are in a form that is suitable for intestinal absorption. In the current study, a simulated gastrointestinal tract was used to compare the bioaccessibility of CsP extracts when encapsulated in liposomes (LipCsP-chitosan and LipCsPs). As indicated in Table 6, there was a significant difference ($P < 0.05$) in bioaccessibility among the tested nanoformulations, which signified that the CsPs were well protected in both chitosan-coated and uncoated systems.

LipCsP-chitosan enhanced the bioaccessibility of CsPs in the gastrointestinal environment. The bioaccessibility of free CsP extract in the gastric phase was 39.65 ± 2.4%, which increased to 74.11 ± 1.3 and 51.08 ± 3.2% when chitosan-coated liposomes

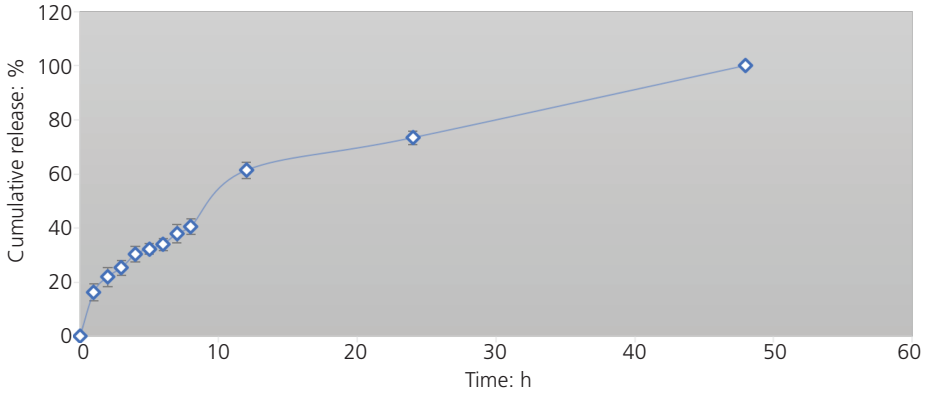

Figure 2. In vitro release of CsPs encapsulated in LipCsP-chitosan in pH 7.4 PBS buffer. Values reported as mean ± standard deviation (n = 3) of three experiments

Table 5. Mathematical kinetic models fitted to investigate the mechanism of CsP release from LipCsP-chitosan

Model	R^2	Equation	Mechanism
Zero order	0.9634	$y = 1.847x + 14.27$	Higuchi diffusion (non-Fickian)
First order	0.8969	$y = -0.04x + 2.089$	
Higuchi	0.9701	$y = 13.619x - 2.8773$	
Korsmeyer–Peppas	0.6431	$y = 0.759x + 0.8036$ $N = 0.7594$	

Table 6. Bioaccessibility of CsPs loaded in nanoformulations in simulated gastric phase and intestinal phase

Formulation	SGF	SIF
CsPs	$39.65^{e} \pm 2.4$	$31.4^{f} \pm 2.8$
LipCsPs	$51.08^{c} \pm 3.2$	$43.71^{d} \pm 3.3$
LipCsP-chitosan	$74.11^{a} \pm 1.3$	$63.32^{b} \pm 5.3$

Note: CsPs, *C. spinarum* polyphenols; LipCsPs, CsP-loaded liposomes; LipCsP-chitosan, chitosan-coated LipCsPs; SGF, simulated gastric fluid; SIF, simulated intestinal fluid. Values are reported as mean ± standard deviation; n = 3. Means followed by dissimilar letters in a row are significantly different from each other at P = 0.05 according to Fisher's LSD

and uncoated liposomes were used for delivery of CsPs, respectively. Conversely, in the intestinal phase, the CsP bioaccessibility increased from 31.4 ± 2.8 to 63.32 ± 5.3 and 43.71 ± 3.3% for LipCsP-chitosan and LipCsP-chitosan, respectively.

The bioaccessibility of CsPs after the intestinal phase differed significantly ($P < 0.05$) from that of the gastric phase. This behavior was attributed to the presence of a mixture of pancreatic enzymes and bile salts that destroyed the liposomal membrane, which was also reported by Hasan *et al*.[40]

The increase in the bioaccessibility of CsPs was attributed to their protection from oxidative degradation in the presence of digestive enzymes in the gastrointestinal environment. The protective function of the delivery systems observed in this study is in agreement with a previous study by Ydjedd *et al*.,[41] who reported on the microencapsulation of carob polyphenols. They reported that the carob polyphenols were effectively protected against pH changes and enzymatic digestion, thereby promoting bioaccessibility in the gut.

The study by Ydjedd *et al*.,[41] however, did not include LipCsP-chitosan. Despite the fact that liposomes have been used as a versatile delivery system for several drugs,[42] their oxidative degradation and physical instability impede their delivery potential. Based on this study, the presence of chitosan adds a protective layer against oxidative degradation in the presence of digestive enzymes. Previously, Hasan *et al*.[40] reported that a chitosan-coated liposome nanodelivery system was able to avoid gastrointestinal enzyme digestion, which further enhanced the bioavailability of active ingredients and agreed with the findings reported in this study. This phenomenon was also mentioned by Panya *et al*.,[43] who reported that chitosan coating on the surface of liposomes reduced lipid oxidation. However, they incorporated rosmarinic acid as an antioxidant, which was combined with chitosan to enhance the reduction of oxidative degradation of liposomes.

3.5 Stability study in simulated environments

The stability of nanoformulations was investigated in simulated environments by evaluating the changes in size and zeta potential of nanoformulations. The negative zeta potential of LipCsPs shown in Table 8 was attributed to the presence of phosphate groups. However, the positive charge displayed by LipCsP-chitosan was due to the adsorbed chitosan on the surface of the liposomes.

There was no significant change in the zeta potential and size of nanoformulations in the oral phase; however, significant differences ($P < 0.05$) in zeta potential and size were observed in the gastric and intestinal phases. The changes in particle size in the gastric phase could be attributed to the swelling of liposomes due to the change in bilayer permeability and osmotic pressure in the presence of hydrochloric acid in the gastric phase, leading to the increased size (Table 7).

The presence of sodium ions caused the discharge of water from the liposome core and caused the shrinkage of the liposomes, hence the reduction in the size of the liposomes. These findings agreed with those of Toro-Uribe *et al*.,[44] who reported on the impact of simulated gastrointestinal fluid (GIF) on the zeta potential and size of liposomes. Based on their study, the acidic gastric phase led to an increase in size due to the alteration of the osmotic potential by hydrochloric acid, while the presence of sodium ions evacuated water from the liposome core and reduced the size of liposomes (Table 7).

The zeta potential in a simulated gastrointestinal environment (Table 8) was affected by the presence of hydrochloric acid in the gastric phase, which altered the ionization state and charge distribution of the phosphatidylcholine head. Furthermore, the anionic bile salts in the intestinal phase increased the magnitude of the negative charge.[34] Slight changes in the size and charge were observed in coated formulations due to the presence of a chitosan layer that withstood the effect of ions on the alteration of the size and charge. The same findings were reported by the study of He *et al*.,[45] where the liposomes were highly affected by acid, bile salts and pancreatic enzymes in the gastrointestinal environment, which triggered their degradation to create payload leakage. Phosphatidylcholine, due to its low phase transition temperature, has a lipid bilayer that is vulnerably destroyed by bile salt. Lipolytic enzymes in pancreatic fluid hydrolyze phospholipids, thereby destroying the liposome structure. Coating liposomes helps overcome the degradation effects in the GIF.[40,46,47] It was reported that the presence of a chitosan layer hinders swelling and release of encapsulated materials.[34]

Furthermore, the electrostatic interaction between chitosan and the lipid bilayer strengthens the structural integrity of the lipid membranes. Another study reported that the stability of chitosan-coated liposomes in SGF was significantly higher as compared with that of uncoated liposomes.[48] Nevertheless, the use of pH-sensitive polymers could help liposomes resist degradation by digestive enzymes and facilitate the release of bioactive compounds in specific parts of the small or large intestines.[49]

3.6 Antimicrobial effect of nanoformulations on bacterial pathogens

The antibacterial activities of CsPs, LipCsPs and LipCsP-chitosan were tested against *K. pneumoniae*. The agar diffusion assay results are shown in Figure 3. The tested nanoformulations exhibited a significant difference ($P < 0.05$) in percent RIZD against *K. pneumoniae*. LipCsP-chitosan exhibited a higher growth inhibition effect as compared with CsPs and LipCsPs. LipCsPs demonstrated significantly greater antimicrobial activity than CsPs ($P < 0.05$). The disparity in antibacterial activity was attributed to the delivery potential of the liposomes. Other studies reported the ability of the lipid bilayer structure to fuse with infectious pathogens and enhance antimicrobial activity as compared with free extracts.[12,50] However, Noudoost *et al*.[51] explained that intermembrane transfer, contact release, absorption, fusion and phagocytosis exhibited by liposomes allowed cellular transport and release of the active component inside the bacterial cell.

Table 7. Stability in the size of nanoformulations in simulated environments of LipCsPs and LipCsP-chitosan

Formulation	Initial	SMF	SGF	SIF
LipCsPs	$176.17^{f} \pm 1.05$	$175.33^{f} \pm 0.76$	$202.00^{c} \pm 1.80$	$165.00^{d} \pm 1.05$
LipCsP-chitosan	$365.22^{e} \pm 0.70$	$364.50^{e} \pm 0.50$	$373.17^{a} \pm 1.26$	$360.83^{b} \pm 1.04$

Note: LipCsPs, *C. spinarum*-polyphenol-loaded liposomes; LipCsP-chitosan, chitosan-coated LipCsPs; SGF, simulated gastric fluid; SIF, simulated intestinal fluid; SMF, simulated mouth fluid;. Values are reported as mean ± standard deviation; $n = 3$. Means followed by dissimilar letters in a row are significantly different from each other at $P \leq 0.05$ according to Fisher's LSD

Table 8. Stability in the zeta potentials of nanoformulations in simulated environments

Nanoformulation	Initial	SMF	SGF	SIF
LipCsPs	$-45.37^{a} \pm 0.78$	$-45.80^{a} \pm 0.26$	$-42.67^{d} \pm 0.58$	$-48.83^{c} \pm 0.76$
LipCsP-chitosan	$+39.30^{b} \pm 0.61$	$+39.13^{b} \pm 1.53$	$+41.00^{f} \pm 1.00$	$+37.50^{e} \pm 0.50$

Note: LipCsPs, *C. spinarum*-polyphenol-loaded liposomes; LipCsP-chitosan, chitosan-coated LipCsPs. Values are reported as mean ± standard deviation; $n = 3$. Means followed by dissimilar letters in a row are significantly different from each other at $P \leq 0.05$ according to Fisher's LSD; SMF, simulated mouth fluid; SGF, simulated gastric fluid; SIF, simulated intestinal fluid

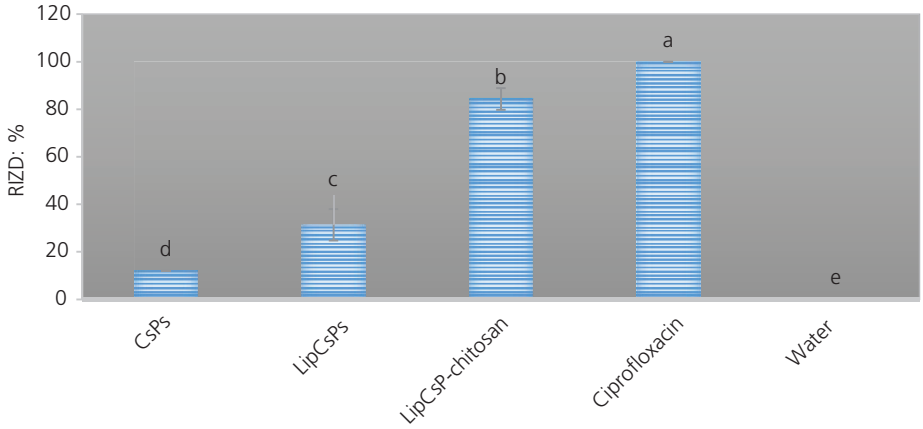

Figure 3. Percent RIZDs against *K. pneumoniae* exhibited by CsPs, LipCsPs and LipCsP-chitosan

At an MIC of 31.25 mg/ml, LipCsP-chitosan reduced the viability of *K. pneumoniae* by 57.45 ± 3.76% after 24 h (Figure 4). An independent study reported that fusion with the bacterial membrane as a result of the fluidity of the lipid bilayer contributes to high antimicrobial doses inside the bacteria. A mimetic property shared by the bacterial cell membrane and the liposomal phospholipid bilayer[52] facilitates fusion with the bacterial wall. Cationic surface modification of liposomes improves their stability, facilitating their antibacterial activity. LipCsP-chitosan showed a higher activity compared with CsPs and LipCsPs. The disparity in antibacterial activity between LipCsP-chitosan and LipCsPs could be due to surface charge. A positively charged coating system has a strong attraction force with the negatively charged membrane of the bacterial cell, causing cell damage. The improved antibacterial activity by positively charged coated liposome systems reported in the present study closely agrees with the results reported by Lee *et al*.[53] However, different materials for surface modification of lipid nanoparticles were used in the study by Lee *et al*.[53] They fabricated lipid-coated hybrid nanoparticles (LCHNPs) composed of a poly(lactic-*co*-glycolic acid) (PLGA) core and a dioleoyl-3-trimethylammonium propane lipid shell and loaded with vancomycin (Van) to form a positively charged liposome system with a zeta potential of +36.13 mV. Another set of lipid nanoparticles was fabricated using Van-PLGA to form a negatively charged nanosystem with a zeta potential of −36.83 mV. When used to treat USA300 biofilms, Van-LCHNPs eradicated up to 99.99% of the underlying biofilm cells, an effect that was not observed with Van and Van-PLGA.

Aligning with this suggestion, the cationic charges of chitosan can interact with negatively charged cell membranes to open tight epithelial junctions.[54] Ammonia (NH_3^+) ions adsorb on microorganism cell walls through electrostatic interaction, leading to cell wall damage and leakage of macromolecules from bacteria.[54] Mady and Darwish[55] suggested that the mucoadhesive properties of chitosan are facilitated by its positively charged surface, which favors adhesions to the cell membrane, which are normally negatively charged.

4. Conclusion

LipCsP-chitosan using lecithin was successfully prepared using the ionic gelation technique. The formulation was fully evaluated for its size, PDI, Z_P, EE% and in vitro release. A bioaccessibility study was conducted, and the formulation showed a high ability to protect CsPs

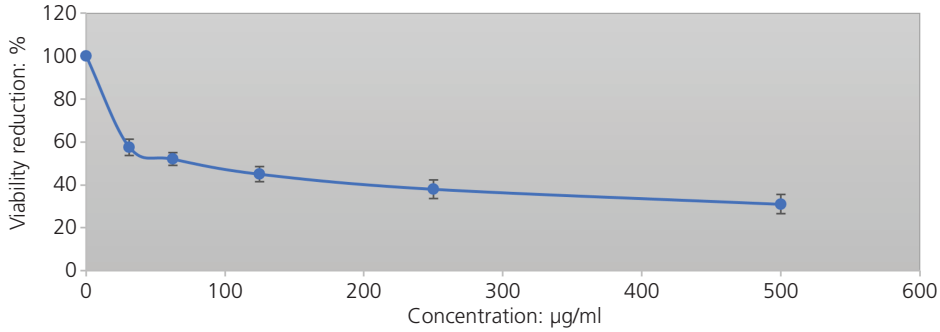

Figure 4. Concentration-dependent viability reduction effect of LipCsP-chitosan. Dissimilar letters in bars indicate significance of viability reduction (%) exhibited by different concentrations

in simulated GIF. The release profile of the CsPs from LipCsP-chitosan was biphasic followed by a sustained release, and the release mechanism was governed by both erosion and diffusion. LipCsP-chitosan exhibited potential antipneumococcal activity against *K. pneumoniae*. The results obtained from this study offer a new approach to the utilization of LipCsP-chitosan as a promising delivery system for antipneumococcal agents.

Acknowledgements

This work was supported by the Centre for Research, Agricultural Advancement, Teaching Excellence and Sustainability in Food and Nutritional Security at the Nelson Mandela African Institution of Science and Technology, Arusha, Tanzania. The authors also acknowledge the following: Infectious Diseases Nanomedicine Laboratory, Department of Pharmaceutical Sciences, Faculty of Natural Sciences, University of the Western Cape, Cape Town, South Africa; Center for Traditional Medicine and Drug Research, Kenya Medical Research Institute, Nairobi, Kenya; and DSI/Mintek Nanotechnology Innovation Centre – Biolabels Node, Department of Biotechnology, University of the Western Cape, Cape Town, South Africa.

REFERENCES

1. Ventola CL (2015) The antibiotic resistance crisis: part 1 causes and threats. *P&T* **40(4)**: 277–283.
2. de Kraker MEA, Stewardson AJ and Harbarth S (2016) Will 10 million people die a year due to antimicrobial resistance by 2050? *PLOS Medicine* **13(11)**: article e1002184.
3. Abeylath SC and Turos E (2008) Drug delivery approaches to overcome bacterial resistance to beta-lactam antibiotics. *Expert Opinion on Drug Delivery* **5(9)**: 931–949.
4. Skwarczynski M, Bashiri S, Yuan Y *et al.* (2022) Antimicrobial activity enhancers: towards smart delivery of antimicrobial agents. *Antibiotics* **11(3)**: article 412.
5. Beyth N, Houri-Haddad Y, Domb A, Khan W and Hazan R (2015) Alternative antimicrobial approach: nano-antimicrobial materials. *Evidence-based Complementary and Alternative Medicine* **2015**: article 246012.
6. Dessie T, Jemal M, Maru M and Tiruneh M (2021) Multiresistant bacterial pathogens causing bacterial pneumonia and analyses of potential risk factors from Northeast Ethiopia. *International Journal of Microbiology* **2021**: article 6680343.
7. Adibkia K, Khorasani G, Payab S and Lotfipour F (2016) Anti pneumococcal activity of azithromycin–Eudragit RS100 nano-formulations. *Advanced Pharmaceutical Bulletin* **6(3)**: 455–459.
8. Zhao C, Xie Y, Zhang F *et al.* (2020) Investigation of antibiotic resistance, serotype distribution, and genetic characteristics of 164 invasive *Streptococcus pneumoniae* from North China between April 2016 and October 2017. *Infection and Drug Resistance* **13**: 2117–2128.
9. Höltje JV and Tomasz A (1975) Specific recognition of choline residues in the cell wall teichoic acid by the *N*-acetylmuramyl-L-alanine amidase of *Pneumococcus*. *Journal of Biological Chemistry* **250(15)**: 6072–6076.
10. Hakenbeck R, Madhour A, Denapaite D and Brückner R (2009) Versatility of choline metabolism and choline-binding proteins in *Streptococcus pneumoniae* and commensal streptococci. *FEMS Microbiology Reviews* **33(3)**: 572–586.
11. Maestro B and Sanz J (2016) Choline binding proteins from *Streptococcus pneumoniae*: a dual role as enzybiotics and targets for the design of new antimicrobials. *Antibiotics* **5(2)**: article 21.
12. Bozzuto G and Molinari A (2015) Liposomes as nanomedical devices. *International Journal of Nanomedicine* **10**: 975–999.
13. Sriwidodo, Umar AK, Wathoni N *et al.* (2022) Liposome–polymer complex for drug delivery system and vaccine stabilization. *Heliyon* **8(2)**: article e08934.
14. Nag M, Lahiri D, Mukherjee D *et al.* (2021) Functionalized chitosan nanomaterials: a jammer for quorum sensing. *Polymers* **13(15)**: article 2533.
15. Vázquez R, Caro-León FJ, Nakal A *et al.* (2021) DEAE–chitosan nanoparticles as a pneumococcus-biomimetic material for the development of antipneumococcal therapeutics. *Carbohydrate Polymers* **273**: article 118605.
16. Berhanu G, Atalel D and Kandi V (2020) A review of the medicinal and antimicrobial properties of *Carissa spinarum* L. *American Journal of Biomedical Research* **8(2)**: 54–58.
17. Ansari I and Patil D (2018) A brief review on phytochemical and pharmacological profile of *Carissa spinarum* L. *Asian Journal of Pharmaceutical and Clinical Research* **11**: 12–18.
18. Fatima A, Singh PP, Agarwal P *et al.* (2013) Treatment of various diseases by *Carissa spinarum* L.: a promising shrub. *International Journal of Pharmaceutical Sciences and Research* **4(7)**: 2489–2495.
19. Mworia J, Gitahi S, Juma K *et al.* (2015) Antinociceptive activities of acetone leaves extracts of *Carissa spinarum* in mice. *Journal of Medicinal and Aromatic Plants* **S1**: article 0006.
20. Harwansh RK, Garabadu D, Rahman MA and Garabadu PS (2010) In vitro anthelmintic activity of different extracts of root of *Carissa spinarum*. *International Journal of Pharmaceutical Sciences and Research* **1(10)**: 84–88.
21. Mundaragi A and Thangadurai D (2018) Process optimization, physicochemical characterization and antioxidant potential of novel wine from an underutilized fruit *Carissa spinarum* L. (Apocynaceae). *Food Science and Technology* **38(3)**: 428–433.
22. Rubaka C, Ndakidemi P, Malebo H and Shahada F (2014) Analysis of phytochemical and antibacterial activity of *Carissa spinarum* Linn crude extracts. *European Journal of Medicinal Plants* **4(8)**: 937–945.
23. Manach C, Scalbert A, Morand C, Rémésy C and Jiménez L (2004) Polyphenols: food sources and bioavailability. *American Journal of Clinical Nutrition* **79(5)**: 727–747.
24. Zhang Q, Xing B, Sun M *et al.* (2020) Changes in bio-accessibility, polyphenol profile and antioxidants of quinoa and djulis sprouts during in vitro simulated gastrointestinal digestion. *Food Science & Nutrition* **8(8)**: 4232–4241.
25. Sonam M, Singh RP and Pooja S (2017) Phytochemical screening and TLC profiling of various extracts of *Reinwardtia indica*. *International Journal of Pharmacognosy and Phytochemical Research* **9(4)**: 523–527.
26. Genwali GR, Acharya PP and Rajbhandari M (2013) Isolation of gallic acid and estimation of total phenolic content in some medicinal plants and their antioxidant activity. *Nepal Journal of Science and Technology* **14(1)**: 95–102.
27. Cheng C, Peng S, Li Z *et al.* (2017) Improved bioavailability of curcumin in liposomes prepared using a pH-driven, organic solvent-free, easily scalable process. *RSC Advances* **7(42)**: 25978–25986.
28. Omwoyo WN, Ogutu B, Oloo F *et al.* (2014) Preparation, characterization, and optimization of primaquine-loaded solid lipid nanoparticles. *International Journal of Nanomedicine* **9**: 3865–3874.
29. Pool H, Quintanar D, Figueroa JDD *et al.* (2012) Polymeric nanoparticles as oral delivery systems for encapsulation and release of polyphenolic compounds: impact on quercetin antioxidant activity & bioaccessibility. *Food Biophysics* **7(3)**: 276–288.
30. Guimarães AC, Meireles LM, Lemos MF *et al.* (2019) Antibacterial activity of terpenes and terpenoids present in essential oils. *Molecules* **24(13)**: 2471.
31. Fraga-Corral M, García-Oliveira P, Pereira AG *et al.* (2020) Technological application of tannin-based extracts. *Molecules* **25(3)**: article 614.

32. Adamczak A, Ożarowski M and Karpiński TM (2020) Antibacterial activity of some flavonoids and organic acids widely distributed in plants. *Journal of Clinical Medicine* **9(1)**: article 109.
33. Kregiel D, Berlowska J, Witonska I *et al.* (2017) Saponin-based, biological-active surfactants from plants. In *Application and Characterization of Surfactants* (Najjar R (ed.)). InTech. London, UK, pp. 183–205.
34. Sebaaly C, Trifan A, Sieniawska E and Greige-Gerges H (2021) Chitosan-coating effect on the characteristics of liposomes: a focus on bioactive compounds and essential oils: a review. *Processes* **9(3)**: article 445.
35. Gibis M, Ruedt C and Weiss J (2016) *In vitro* release of grape-seed polyphenols encapsulated from uncoated and chitosan-coated liposomes. *Food Research International* **88(Part A)**: 105–113.
36. Abosabaa SA, Arafa MG and ElMeshad AN (2021) Hybrid chitosan–lipid nanoparticles of green tea extract as natural anti-cellulite agent with superior in vivo potency: full synthesis and analysis. *Drug Delivery* **28(1)**: 2160–2176.
37. Baranauskaite J, Duman G, Corapcıoğlu G *et al.* (2018) Liposomal incorporation to improve dissolution and stability of rosmarinic acid and carvacrol extracted from oregano (*O. onites* L.). *BioMed Research International* **2018**: article 6147315.
38. Lisperguer J, Saravia Y and Vergara EV (2016) Structure and thermal behavior of tannins from *Acacia dealbata* bark and their reactivity toward formaldehyde. *Journal of I Chilean Chemical Society* **61**: 3188–3190.
39. Liang J, Li F, Fang Y *et al.* (2011) Synthesis, characterization and cytotoxicity studies of chitosan-coated tea polyphenols nanoparticles. *Colloids and Surfaces B: Biointerfaces* **82(2)**: 297–301.
40. Hasan M, Elkhoury K, Kahn CJF, Arab-Tehrany E and Linder M (2019) Preparation, characterization, and release kinetics of chitosan-coated nanoliposomes encapsulating curcumin in simulated environments. *Molecules* **24(10)**: article 2023.
41. Ydjedd S, Bouriche S, López-Nicolás R *et al.* (2017) Effect of in vitro gastrointestinal digestion on encapsulated and nonencapsulated phenolic compounds of carob (*Ceratonia siliqua* L.) pulp extracts and their antioxidant capacity. *Journal of Agricultural and Food Chemistry* **65(4)**: 827–835.
42. Nakhaei P, Margiana R, Bokov DO *et al.* (2021) Liposomes: structure, biomedical applications, and stability parameters with emphasis on cholesterol. *Frontiers in Bioengineering and Biotechnology* **9**: article 705886.
43. Panya A, Laguerre M, Lecomte J *et al.* (2010) Effects of chitosan and rosmarinate esters on the physical and oxidative stability of liposomes. *Journal of Agricultural and Food Chemistry* **58(9)**: 5679–5684.
44. Toro-Uribe S, Ibáñez E, Decker EA and McClements DJ (2018) Design, fabrication, characterization, and in vitro digestion of alkaloid-, catechin-, and cocoa extract-loaded liposomes. *Journal of Agricultural and Food Chemistry* **66(45)**: 12051–12065.
45. He H, Lu Y, Qi J *et al.* (2019) Adapting liposomes for oral drug delivery. *Acta Pharmaceutica Sinica B* **9(1)**: 36–48.
46. Lee MK (2020) Liposomes for enhanced bioavailability of water-insoluble drugs: in vivo evidence and recent approaches. *Pharmaceutics* **12(3)**: article 264.
47. Zamani-Ghaleshahi A, Rajabzadeh G, Ezzatpanah H and Ghavami M (2020) Biopolymer coated nanoliposome as enhanced carrier system of perilla oil. *Food Biophysics* **15(3)**: 273–287.
48. Filipović-Grcić J, Skalko-Basnet N and Jalsenjak I (2001) Mucoadhesive chitosan-coated liposomes: characteristics and stability. *Journal of Microencapsulation* **18(1)**: 3–12.
49. Pimentel-Moral S, Verardo V, Robert P, Segura Carretero A and Martinez-Ferez A (2016) Nanoencapsulation strategies applied to maximize target delivery of intact polyphenols. In *Encapsulations* (Grumezescu AM (ed.)). Elsevier. Amsterdam, the Netherlands, pp. 559–595.
50. Wang Z, Ma Y, Khalil H *et al.* (2016) Fusion between fluid liposomes and intact bacteria: study of driving parameters and in vitro bactericidal efficacy. *International Journal of Nanomedicine* **11**: 4025–4036.
51. Noudoost B, Noori N, Abedini G *et al.* (2015) Encapsulation of green tea extract in nanoliposomes and evaluation of its antibacterial, antioxidant and prebiotic properties. *Journal of Medicinal Plants* **14**: 66–78.
52. Wang DY, van der Mei HC, Ren Y, Busscher HJ and Shi L (2020) Lipid-based antimicrobial delivery-systems for the treatment of bacterial infections. *Frontiers in Chemistry* **7**: article 872.
53. Lee HW, Kharel S and Loo SCJ (2022) *Lipid-coated Hybrid Nanoparticles for Enhanced Bacterial Biofilm Penetration and Antibiofilm Efficacy*. Research Square, Durham, NC, USA.
54. Imam SS, Alshehri S, Altamimi MA *et al.* (2022) Formulation of chitosan-coated apigenin bilosomes: in vitro characterization, antimicrobial and cytotoxicity assessment. *Polymers* **14(5)**: article 921.
55. Mady MM and Darwish MM (2010) Effect of chitosan coating on the characteristics of DPPC liposomes. *Journal of Advanced Research* **1(3)**: 187–191.